Continental Shelf Research 31 (2011) 85–97

Contents lists available at ScienceDirect

Continental Shelf Research

journal homepage: www.elsevier.com/locate/csr

A buoyant plume adjacent to a headland—Observations of the Elwha River plume

Jonathan A. Warrick*, Andrew W. Stevens

U.S. Geological Survey, Pacific Coastal and Marine Science Center, 400 Natural Bridges Dr., Santa Cruz, CA 95062, USA

ARTICLE INFO

Article history:
Received 12 March 2010
Received in revised form
12 November 2010
Accepted 19 November 2010
Available online 2 December 2010

Keywords:
River plume
Coastal headland
Strait of Juan de Fuca
Elwha River
Dam removal

ABSTRACT

Small rivers commonly discharge into coastal settings with topographic complexities – such as headlands and islands – but these settings are underrepresented in river plume studies compared to more simplified, straight coasts. The Elwha River provides a unique opportunity to study the effects of coastal topography on a buoyant plume, because it discharges into the Strait of Juan de Fuca on the western side of its deltaic headland. Here we show that this headland induces flow separation and transient eddies in the tidally dominated currents (O(100 cm/s)), consistent with other headlands in oscillatory flow. These flow conditions are observed to strongly influence the buoyant river plume, as predicted by the "small-scale" or "narrow" dynamical classification using Garvine's (1995) system. Because of the transient eddies and the location of the river mouth on the headland, flow immediately offshore of the river mouth is directed eastward twice as frequently as it is westward. This results in a buoyant plume that is much more frequently "bent over" toward the east than the west. During bent over plume conditions, the plume was attached to the eastern shoreline while having a distinct, cuspate front along its westernmost boundary. The location of the front was found to be related to the magnitude and direction of local flow during the preceding O(1 h), and increases in alongshore flow resulted in deeper freshwater mixing, stronger baroclinic anomalies, and stronger hugging of the coast. During bent over plume conditions, we observed significant convergence of river plume water toward the frontal boundary within 1 km of the river mouth. These results show how coastal topography can strongly influence buoyant plume behavior, and they should assist with understanding of initial coastal sediment dispersal pathways from the Elwha River during a pending dam removal project.

Published by Elsevier Ltd.

1. Introduction

Buoyant (hypopycnal) plumes are a primary pathway for the dispersal of river water and dissolved materials into the coastal ocean (Wright and Coleman, 1971; Garvine, 1974). Buoyant plumes also influence the dispersal of suspended sediment from rivers, although suspended sediment will settle quickly downward from these surface-bound buoyant plumes and advect according to particle settling characteristics and water column and bottom boundary layer conditions (Kineke et al., 2000; Mertes and Warrick, 2001; Geyer et al., 2004; Wright and Friedrichs, 2006; Milligan et al., 2007; Hill et al., 2007). Owing to the influence of buoyant river plumes on coastal water quality, ecosystems, and circulation, there have been substantial efforts and achievements in trying to understand the physical behavior of these plumes and their fronts with respect to river discharge, the Coriolis effect, and tidal and meterologic conditions (e.g., Garvine and Monk, 1974; Luketina and Imberger 1987; O'Donnell, 1990; Gelfenbaum and Stumpf, 1993; Garvine, 1995; O'Donnell et al., 1998; Fong and Geyer, 2001; MacDonald and Geyer, 2004; Hetland, 2005; Piñones et al., 2005; Whitney and Garvine, 2005; Pritchard and Huntley, 2006; Chen et al., 2009; Hickey et al., 2010; Kilcher and Nash, 2010).

The majority of river plume investigations have focused on relatively simple physical settings, such as those with straight shorelines and topographic contours (e.g., O'Donnell, 1990; Yankovsky and Chapman, 1997; Fong and Geyer, 2002; Pritchard and Huntley, 2006; MacDonald et al., 2007; Hickey et al., 2010), which has allowed for exploration of the plume without overly complicated influence from topography. Coastal settings are inherently complex, however, with physical features such as islands, embayments and headlands, which can strongly influence coastal circulation and sediment transport (Wolanski and Hamner, 1988; Signell and Geyer, 1991; McCabe et al., 2006). There are very few observations of buoyant river plumes in these more complex topographic settings – one exception is Piñones et al., 2005 – even though many of the world's smaller, yet geochemically important (Milliman and Syvitski, 1992; Wheatcroft et al., 2010), rivers reside in active tectonic settings with irregular coastlines.

* Corresponding author. Tel.: +1 831 427 4793.
E-mail address: jwarrick@usgs.gov (J.A. Warrick).

0278-4343/$ - see front matter Published by Elsevier Ltd.
doi:10.1016/j.csr.2010.11.007

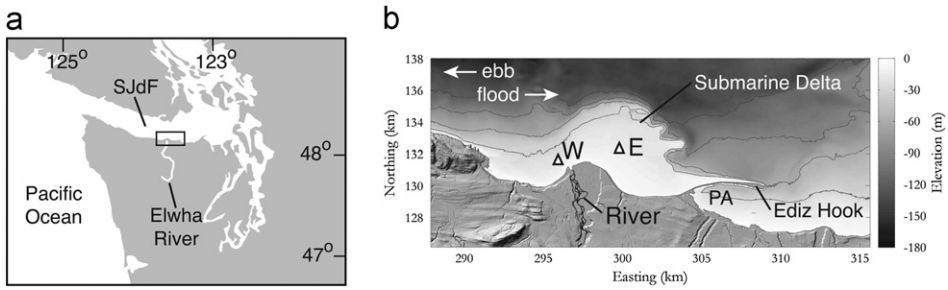

Fig. 1. The study site and measurement locations of the Elwha River plume: (a) the Elwha River discharges into the Strait of Juan de Fuca (SJdF), (b) the local topography and bathymetry of the Elwha River delta. The locations of the western and eastern (W,E) ADCP sites are shown with triangles. The general flow direction of the tidal floods and ebbs are shown with arrows. Isobaths are shown at 30 m increments from mean sea level. The map projection is Washington State Plane North (NAD83) and the vertical datum is NAVD88.

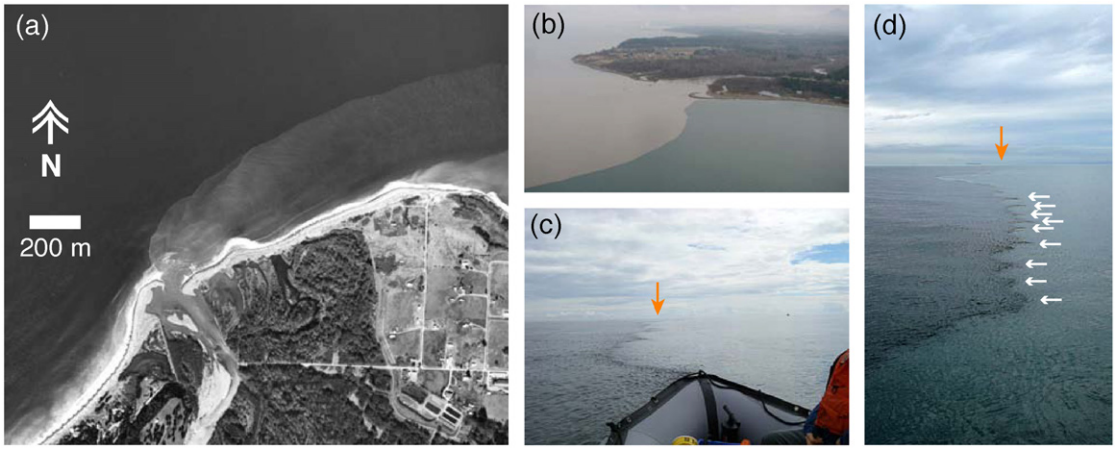

Fig. 2. Photographs of the Elwha River buoyant plume: (a) a 1994 aerial photo showing the turbid plume during river discharge of 32 m^3/s and (b) oblique aerial photo of the highly turbid plume on 11 December 2007 at 13:30 Pacific Standard Time (PST) immediately after river flooding. (c) and (d) The plume front as observed on 9 June 2007 at 18:30 Pacific Daylight Time (PDT) and shown with an orange arrow. The buoyant plume is to the right of the front in both photos. White arrows identify cusp-like indentations with horizontal spacing of ~2 m. (photo credits: a—Washington DNR ; b—US Coast Guard; c—Jon Warrick; and d—Andrew Stevens). (For interpretation of the references to colour in this figure legend, the reader is referred to the web version of this article.)

The purpose of this paper is to build upon the knowledge of buoyant plumes in complex settings by evaluating the effects of a coastal headland on the behavior of a river plume. We focus on the plume of the Elwha River, which exists along the southern shore of the Strait of Juan de Fuca and forms on the western side of this river's deltaic headland (Figs. 1 and 2). Our plume observations were made to describe the patterns and dynamics of the plume within ~1 km of the river mouth, owing to the importance of this initial region to plume formation and sediment dispersal, which are relevant to the potential effects of a pending dam removal project in the Elwha River watershed described below.

After presenting information about the physical setting and data collection efforts, we focus on both (a) the effects of the headland on circulation around the delta and (b) how the plume responds to these circulation patterns. These two research goals were addressed by two phases of field research: (i) a 96-day deployment of two acoustic Doppler current profilers (ADCP) offshore of the river mouth delta in early 2006 and (ii) several days of detailed measurements of the buoyant river plume during the summer freshet of 2007.

2. Setting

The Elwha River watershed (831 km^2) originates in the Olympic Mountains of Washington (Fig. 1), and two dams interrupt this discharge on its way to the southern Strait of Juan de Fuca. These dams, which trap sediment from over 90% of the watershed drainage area, have produced significant reductions in sediment supply to the lower river and the coast (Randle et al., 1996; Kloehn et al., 2008; Warrick et al., 2009). The most recent estimate of sedimentation in the reservoirs was made in 1995, when 13.5 million m^3 of sediment was measured and estimated to be roughly 50% silt and clay and 50% sand, gravel and cobble (Gilbert and Link, 1995; Childers et al., 2000). A pending dam removal project by the US Department of Interior is intended to restore salmon spawning habitat and sediment transport through the lower river and coastal zone in the coming decade, during which sediment loading to the Strait should exceed present rates by several orders of magnitude (Wunderlich et al., 1994; Duda et al., 2008; Konrad, 2009).

Water discharge from the Elwha River averages approximately 40 m^3/s, although there is significant seasonal and storm variability (Fig. 3). The annual hydrograph can be characterized as having a late spring freshet from upland snowmelt, receding baseflow during the summer resulting in the lowest discharge rates on average during late summer, and winter precipitation events that induce higher flows and the largest hydrologic events for the river (Fig. 3). The two dams on the river do little to affect these discharge conditions, as they are largely operated as "run of the river" (Duda et al., 2008). The peak river discharge rate during an "average" annual flood (defined here to be the 2-yr recurrence interval peak instantaneous discharge) is approximately 400 m^3/s based on a 93-yr record from the US Geological Survey (USGS) river gauge 12045500 (Elwha River at McDonald Bridge), and maximum discharge rates during this record are estimated to be ~1000 m^3/s.

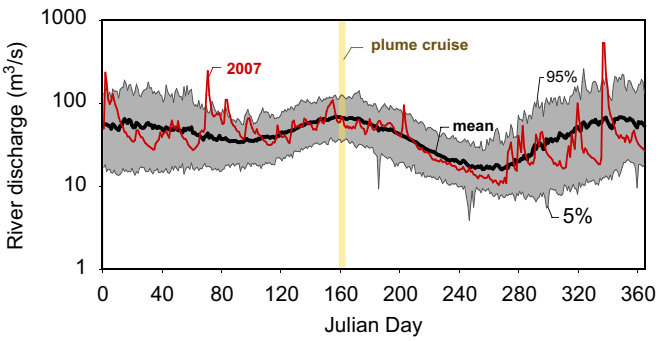

Fig. 3. Discharge statistics for the Elwha River compared to discharge conditions during 2007. The dates of the 2007 plume cruise are also highlighted. Daily mean and percentiles (5% and 95%) based on 91 years of daily means from the USGS gauge no. 12045500 (Elwha River at McDonald Bridge).

The Elwha River delta has a sinuous planform shape that protrudes approximately 2 km into the Strait of Juan de Fuca (Fig.1b). A similar pattern is observed in the submarine portion of the delta, for which a bathymetric high extends several km into the Strait (Fig. 1b). The Strait of Juan de Fuca, in turn, is the primary channel connecting Puget Sound and Georgia Basin to the Pacific Ocean. Owing to the tidal conditions and riverine discharges into these water bodies, surface currents in the midchannel of the Strait are dominated by O(100) cm/s tidal currents and O(10) cm/s residual currents toward the Pacific (Holbrook et al., 1980; Thomson et al., 2007). It is also recognized that the residual currents of the Strait have three-dimensional baroclinic motions that vary significantly at fortnightly and seasonal timescales and spatially across the channel (Masson and Cummins, 2004; Thomson et al., 2007).

Other relevant physical and meteorological conditions of the study area follow. The tides of the Port Angeles ("PA" in Fig. 1b) are mesotidal with a spring tidal range of 2.15 m, and they are mixed, predominately diurnal. The wave regime is dominated by northwesterly swell originating from the Pacific Ocean and locally generated wind waves from the Strait, although significant wave heights are generally less than 0.5 m, which are substantially smaller than those observed on the outer Pacific coast (Warrick et al., 2009). The Elwha River delta is in the lee of the Olympic Mountains, which limits the effects of strong southerly winds from the recurring storms of the winter (Lange, 1999, 2003). Therefore, the strongest and most common winds of the Elwha River delta region tend to be sea breeze from Pacific Ocean (i.e., westerlies), which peak during the summer, but can also occur during winter storms (Lange, 1999, 2003).

3. Field studies

3.1. ADCP observations—winter–spring 2006

Two instrumented frames were deployed in 15 m water depth on the east and west side of the river mouth ("E" and "W" in Fig. 1b) between 27 January and 3 May 2006, resulting in a 96-day deployment. Each frame was equipped with an upward-looking 1200 kHz acoustic doppler current profiler (ADCP) that was mounted 0.6 m above the seafloor. Profiles of current velocity were recorded at 15-min intervals from 1.8 m above the bottom to the water surface with a vertical resolution of 0.75 m. Values above the water surface were removed from the record based on data from the ADCP's pressure sensor using the equations described in Saunders (1981). Waves were also recorded, and these data are summarized by Warrick et al. (2009).

3.2. Plume cruise observations

Detailed plume observations were made between 8 and 12 June 2007, during which time the river discharge averaged 60 m^3/s at the USGS gaging site (Fig. 3). An upward-looking 1200 kHz ADCP was deployed on 8 June 2007 in 8.5 m water depth approximately 400 m northwest of the river mouth. This site was located approximately 240 m southeast of the West ADCP Site from the winter of 2006. Profiles of current velocity were recorded at 5-min intervals from 3.0 m above the bottom to the water surface with a vertical resolution of 0.5 m. Measurements above the water surface were removed as described above, and this ADCP was recovered on 12 June 2007.

Repeat measurements of the position of the plume front at the surface were collected using a small inflatable skiff and a Garmin 60Csx handheld GPS with a horizontal accuracy of ± 5 m. For each measurement, the boat operator located the point nearest the river mouth where the plume front was visually identifiable (usually a foam line and an abrupt change in water color and clarity). The boat operator positioned the boat immediately adjacent to the front and moved away from the river mouth, following the plume front until it was no longer clearly visible. At the same time a handheld GPS recorded the position at 5-s intervals. Example photos of the plume front from this operation are shown in Fig. 2c and d.

Spatial variations in the surface temperature and salinity were characterized using a profiling and inductive FSI conductivity temperature depth (CTD) sensor used in two different ways. Firstly, CTD profiles of temperature and salinity were measured repeatedly along two cross-shore transects on either side of the river mouth on 9 June 2007. The transects consisted of 8 (west) or 9 (east) stations and extended roughly 500 m offshore in water depths ranging from 3 to 12.5 m. Only data from the down-cast portion of the profile were used for analyses. Secondly, on 11 June 2007 the CTD was pole-mounted 0.5 m off the bow of the R/V *Karluk* at roughly 0.4 m below the surface. Continuous measurements of temperature and salinity were recorded as the vessel navigated along a survey grid that extended 1 km in the alongshore direction and 1.5 km offshore and included 4 across-shore transects. While underway, the position of the boat was recorded using a Garmin GPSMAP 3006C with a horizontal accuracy of ± 5 m. We did not make field observations on 10 June 2007 owing to strong westerly winds and unfavorable sea-state conditions. All data were referenced to local Pacific Daylight Time (PDT), which is equivalent to 7 h subtracted from Coordinated Universal Time (UTC).

4. Results

4.1. Observations of circulation around the delta

Flow around the delta is observed to be both unsteady in time and non-uniform in space. Tidal harmonics explain the majority of the variance in both depth-averaged current records (84% and 90%), and the dominant harmonic is M2 (semidiurnal), with significant contributions from K1, O1, S2, and N2 (Table 1). We note that the M2-dominated harmonics are similar to those reported for the central Strait of Juan de Fuca by Foreman et al. (2004), who suggest that the major ellipse axes are $\sim$50 and $\sim$25 cm/s for M2 and K1, respectively. There are significant differences in the amplitudes of these tidal harmonics between our two sites, however, and on average the West site amplitudes are approximately half those measured at the East site (Table 1).

Tidal flows were dominantly observed in the alongshore direction, as may be expected, shown by the major axes of principle component analyses (Fig. 4). Because of the shape of the delta, these components are roughly orthogonal to each other ($\sim$70°), even

Table 1
A summary of the harmonic (i.e., tidal) components of depth-averaged currents offshore of the Elwha River delta. The harmonic constituents of the Port Angeles, WA tidal gauge are shown for comparison.

Constituent	W Site ADCP Major axis amplitude (cm/s)	E Site ADCP Major axis amplitude (cm/s)	Port angeles, WA (9444090) Amplitude (cm)
M2	23.3	69.5	51.4
K1	11.7	25.2	66.7
O1	11.2	14.6	39.1
S2	6.9	22.5	14.6
N2	5.7	15.1	11.6
Remaining constituents	All < 5 cm/s	All < 5.5 cm/s	All but SA and P1 are < 10 cm
Total variance predicted (%)	84	90	

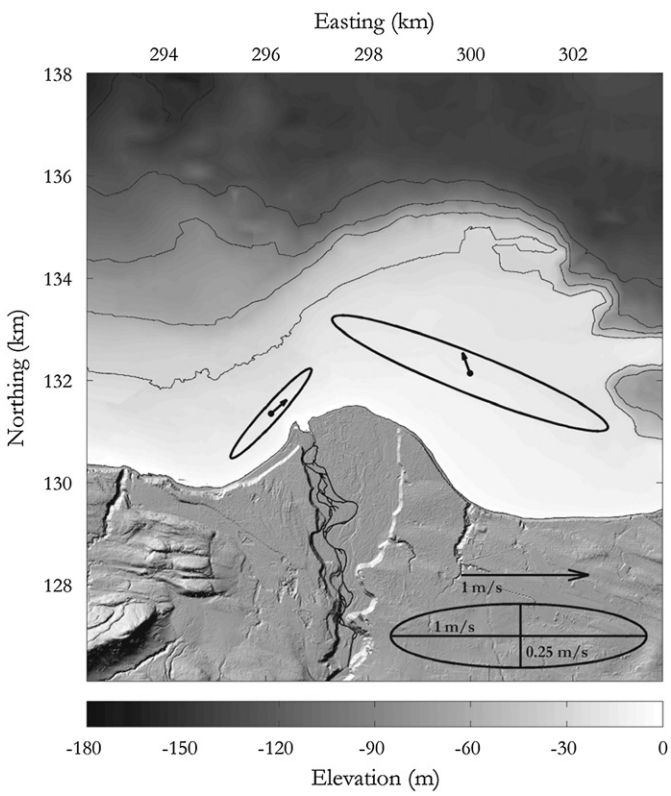

Fig. 4. The mean residual current (arrow) and the major and minor axes of the principle components (ellipses) of depth-averaged currents during winter 2006.

though the stations were less than 4 km apart (Fig. 4). However, the amplitude of these major axes differed by a factor greater than 2, as they were 47 and 116 cm/s for the West and East site, respectively. We note that there is little vertical variance in the amplitude or direction of tidal or principle component analysis parameters beyond an excepted shear in current velocities near the bed.

The West and East sites have residual currents of 16 and 17 cm/s, respectively, although there is 69° difference in the direction of these currents, resulting in net convergence and offshore transport of these residual currents between the two sites (Fig. 4). The residual currents at the West site are approximately parallel to the alongshore currents. This result is caused by strong flood-like direction flow in over 70% of the observations at this site (e.g., see histogram in Fig. 5a). Residual currents at the East site have significant alongshore (toward the Pacific Ocean) and across-shore (directed offshore) components (Fig. 4).

Although currents at the West and East sites were strongly tidal, there is generally very little correlation between the alongshore components of the currents between these sites (Fig. 5). For example, at zero time-lag, the two sites are positively correlated with an r^2 of only 0.28 (Fig. 5a). This is partly owing to converging alongshore currents (upper left panel of Fig. 5a) when the East site experiences its strongest ebbing currents (i.e., > 100 cm/s). Converging conditions were observed during a third of the sampling record (Fig. 5a). The scatter in this relationship is also attributed to a regular hysteresis or looping observed in the data, represented by the arrow in Fig. 5a. A clockwise hysteresis (using the reference frame shown in Fig. 5a) was observed in over 90% of the records when diurnal subsets of the data were compared. Thus, there are significant differences in the currents at these two sites during flooding and ebbing conditions.

These differences can be characterized with cross-correlation analyses (Fig. 5b and c). For these analyses we considered two conditions – flooding and ebbing – as defined by the East site. During flooding, alongshore currents were positively correlated with a peak correlation (r) of 0.63 for a lag of 0.75 h (Fig. 5b). Ebbing, in contrast, shows weak negative correlation at zero-lag and a stronger negative correlation during the latter portion of the ebb (the minimum r of −0.5 to −0.65 occur at lags of 2.5 to 6.5 h; Fig. 5c). This negative correlation during the latter portion of the ebb is characterized by converging alongshore flow described above (Fig. 5a).

In summary, there are strong oscillatory flows and significant residual flows in the coastal section of the Strait of Juan de Fuca where the Elwha River discharges. Immediately offshore of the river mouth, there is strong asymmetry in the currents, for which flood-directed conditions occur over twice as frequently as ebb-directed currents (Fig. 5a). Below we suggest that the patterns and characteristics described above are caused by flow-separation and transient eddies formed by the delta headland, and we show that these conditions strongly influence the river plume and its front.

4.2. Flow around the delta headland

As shown above the circulation in the vicinity of the Elwha River delta is strongly tidal, and yet there is strong flow asymmetry and significant spatial differences between the alongshore flow during flooding and ebbing conditions. These observations are qualitatively consistent with flow separation and eddy generation at the delta headland in this oscillatory flow (Geyer and Signel, 1990; Signell and Geyer, 1991; McCabe et al., 2006). Here we use quantitative methods to evaluate circulation along the Elwha delta to better characterize whether these transient features may influence the river plume.

Signell and Geyer (1991) provide a framework for understanding flow separation and transient eddy formation in oscillatory coastal flows. One characteristic of these systems is that the tidal excursion length must be equivalent to or longer than the headland length scale. For M2 tidal currents with amplitude of 70 cm/s (Table 1), the tidal excursion is approximately 10 km, which

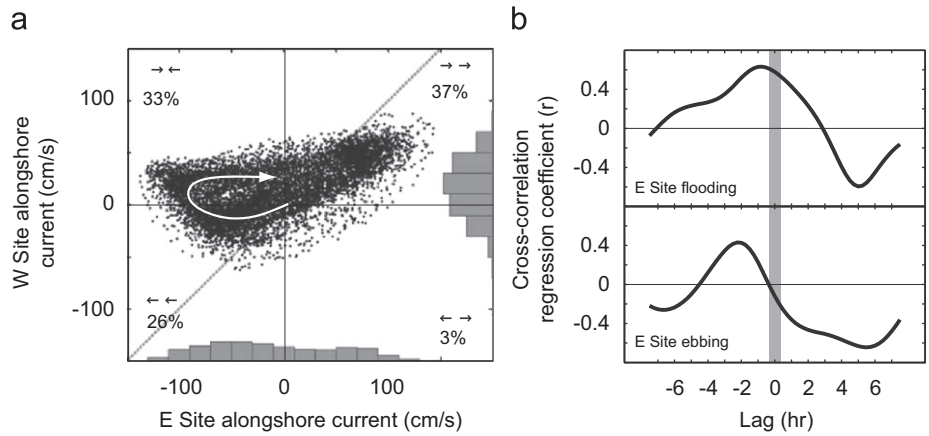

Fig. 5. Comparison of the depth-averaged alongshore currents between the two ADCP sites: (a) comparison of currents, including histograms of current velocities along figure axes. The percentages shown are the frequency of observations within each of the figure's quadrants. Arrows above the percentages represent the direction of the West (left) and East (right) alongshore current velocities. The white arrow represents the hysteresis loop observed in the majority of the observations. (b) and (c) The cross-correlation relationship between the two alongshore current records, although considered only for (b) flooding currents at the E Site and (c) ebbing currents at the E Site.

certainly exceeds the 2–5 km length scale of the Elwha River delta headland (Fig. 2).

Secondly, the potential for flow separation can be assessed using the momentum equation. As flow must accelerate toward a headland and decelerate after the headland, a minimum in the pressure field is formed at the tip owing to the Bernoulli effect (Signell and Geyer, 1991). If flow is strong and the headland is adequately sharp in shape, an adverse – or reversing – pressure gradient will be formed immediately downstream of the headland tip, which will induce flow separation and opposing flows in the headland lee. By considering somewhat simplified physical conditions, Signell and Geyer (1991) suggest that a significant adverse pressure gradient can occur when advection (A) dominates both friction (F) and local acceleration (P) in the momentum equation for the region of flow separation. This will be highly dependent upon the headland shape (S), as shown by the following ratios (after Eqs. (16) and (17) in Signell and Geyer, 1991):

$$\frac{A}{F} \sim \frac{H}{C_D a} S \tag{1}$$

$$\frac{A}{P} = \frac{U_o}{\sigma a} S \tag{2}$$

where H is offshore water depth, C_D is the coefficient of drag, a is the offshore length scale of the headland, S is the headland shape factor ($S=(\alpha^2+\alpha)/3$, where α is the ratio of the offshore (a) and alongshore (b) length scales), U_o is the far-field flow magnitude, and σ is the frequency of oscillation in the flow.

Applying this framework to the Elwha River delta, we find that a and b are both approximately 2 km, which results in α of $\sim$1 and $S\sim$0.7. We note that this places the Elwha River delta at the lower limit, or least pronounced, of headlands for which this theory was developed, but we proceed owing to the strong results that follow. We also suggest that H is 20–30 m, C_D is $\sim 2.5\times10^{-3}$ (after Signell and Geyer, 1991), U_o is $\sim$1 m/s, and σ is $\sim 2.3\times10^{-5}\ \mathrm{s}^{-1}$ (semi-diurnal). Applying these to Eqs. (1) and (2), we find that

$$\frac{A}{F} \sim 3\text{–}4 \ \text{ and } \ \frac{A}{P} \sim 15$$

which are conditions for which flow separation and transient eddies would be regular features on all tides as suggested by Signell and Geyer (1991).

Although Signell and Geyer (1991) suggest that these scaling parameters can also be used to further describe eddy behavior (e.g., propagation and number of eddies), we note that there are additional characteristics of the Elwha River delta that should be considered before a better understanding of circulation for the region can be developed. For example, the submarine portion of the delta and the coastal irregularities on both sides of the delta (Fig. 1b) are obstacles that water must flow over and around, and a better accounting of the effects of these features – including their effects on water masses, sea surface elevations, and associated form drag (cf. McCabe et al., 2006) – will be needed to further characterize flow in the river plume region. Regardless, the data and discussion above clearly show that: (i) flow separation and transient eddies are regular features for the tidal oscillations that dominate the local currents, (ii) the western location of the river mouth with respect to the deltaic headland subjects the near-field plume to reversing flow during regional ebbs owing to a headland-induced eddy, and (iii) this condition results in strong asymmetry in alongshore flow in this near-field plume region shown by greater frequency of flood-directed (or eastward) currents and significant net flow (Figs. 4 and 5a).

4.3. Observations of the plume front

Detailed measurements of the plume and its front were made in June 2007, and the observations of flow near the river mouth during these cruises are shown in Fig. 6. During this interval of time, flow is dominantly directed toward the northeast with brief (4–6 h) reversals in direction (Fig. 6a). Peak flow speeds were 75 cm/s, and there is little shear in the vertical velocity structure during speeds in excess of 25 cm/s (Fig. 6b and c).

Two time-series of the westernmost plume front during this time are shown in Fig. 7. No easternmost front was observed during these measurements, which suggests that the plume was attached to the eastern shoreline. The first set of mapped fronts was collected during accelerating alongshore flow, and the front progressively bent over toward the eastern shoreline (Fig. 7a–c). The second set of fronts (Fig. 7d–f) represents conditions during decelerating alongshore flow. Unfortunately, neither set of front observations characterized conditions when flow was ebb-like (i.e., toward the west). Regardless, these front observations provide insights into the behavior of the plume under different unsteady conditions.

On 9 June 2007 the westernmost front was initially weakly defined and difficult to track (blue lines, Fig. 7a). However, as the alongshore flow strengthened, the front became easily recognizable owing to its color, flow convergence, and 2–4 m cusp-like indentations (Fig. 2c and d), and it proceeded to shift toward the east (Fig. 7a). Small (0.1–1.0 m) eddies were observed within

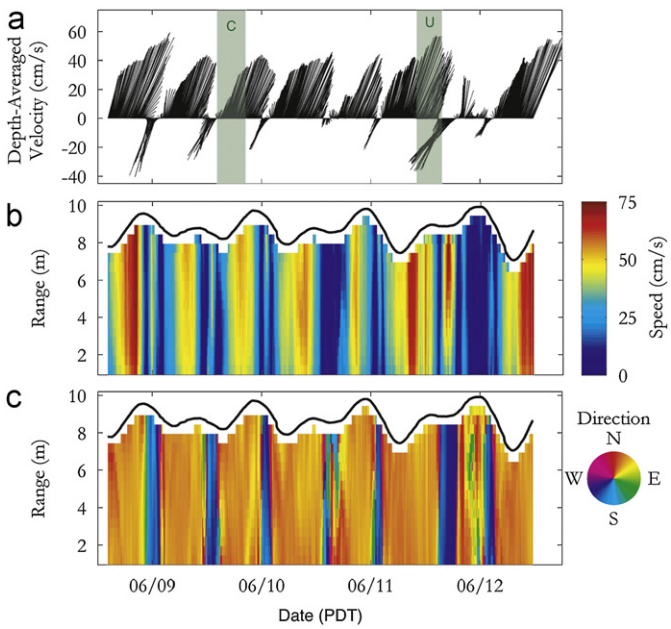

Fig. 6. General conditions and observations made during the 2007 plume study. (a)–(c) Water level and velocity measurements made at the moored ADCP site W. Times of the detailed plume and plume front observations are highlighted with bars in (a) and the style of CTD sampling is denoted with a letter (c—casts and u—underway).

the cusp-like indentations along the front, indicative of vigorous mixing (cf. Trump and Marmorino, 2003). Similar cuspate features were observed at the plume front during 11 June 2007, when the plume relaxed toward the west (Fig. 7d).

To evaluate the relation between the position of the front and alongshore flow, we measured the time-dependent direction of the front with respect to the river mouth. For these measurements, the alongshore direction was defined to be 55° NE with the across-shore direction orthogonal. Direction to the front was measured at regular distances from the river mouth bar, which is identified by a dot in Fig. 7a. An example of the results of these measurements is shown in Fig. 8a, where the direction to the front is shown for a distance 500 m offshore of the shoreline. We note that front positions were measured at several alongshore distances (200–700 m), and the general patterns and implications of the results presented below were not sensitive to these modifications. Perhaps the most important result of these measurements is that the location of the plume front is shown to be related to the surface water alongshore current velocity, i.e., the plume was more "bent over" during higher alongshore velocities. However, for the same speed there are substantial differences in the front position during the accelerating and decelerating flow observations (Fig. 8a). Thus, the plume appears to exhibit a hysteresis, or looping, behavior in its relation between alongshore current and position.

Owing to the fact that hysteresis patterns are commonly related to "memory" in a system (Bertotti and Mayergoyz, 2006), we investigated whether a preceding mean alongshore current speed would better describe the plume front position during both accelerating and decelerating flow. It was found that a 75-min preceding window produced the maximum overlap in front position for the contrasting flow conditions (Fig. 8b). This observation is consistent with – although also partially dependent upon – the unsteady plume front position during steady (~50 cm/s) currents on 9 June (Fig. 8a). The final four mapped plume fronts (green through red; Fig. 7a) were obtained during steady alongshore-current speeds of 47–50 cm/s; however, the front position was observed to move ~30° downcoast during the 80 min during which these observations were made (Fig. 8a). Thus, during an interval of steady flow the plume position continued to be unsteady for over an hour. We note that this O(1 h) time scale is equivalent to the time scale of a perturbation in the front, which can be approximated by the ratio of the length of the observed front (~1 km) to the along-front water parcel velocity during the conditions observed (approximated to be 20–50 cm/s as detailed below), i.e., 0.6–1.4 h.

We also highlight that the plume front position propagated westward (i.e., into the flow) on 11 June when the alongshore flow continued to flood (Fig. 7d). To propagate against this flow, we note that the alongshore component of the velocity induced by the freshwater-induced baroclinic anomaly must have exceeded the alongshore flow velocity. We investigate these patterns of salinity and buoyancy in the next section.

4.4. Observations of plume salinity

Continuous measurements of surface water salinity on 11 June show reduced salinity related to the river plume and its front (Fig. 9). Outside of the plume the salinity averaged 31.3 ± 0.2 psu, and sharp 3–5 psu gradients were observed at the plume front at ~0.4 water depth. We observed the low salinity water to be strongly bent over to the east of the river mouth, consistent with front mapping observations on this day (cf. Fig. 7d). Closer examination of the across-shore transects through the front show strong salinity gradients at the front, which existed over distances of less than 5 m. We also often observed a 15–30 m wide region of local minimum in the salinity immediately behind the front (Fig. 10), which we characterize as the plume head (cf. O'Donnell, 1993). These data also reveal substantial differences in the salinity structure within the plume (shading; Fig. 10). Along transect III, which is nearest to the river mouth (cf. Fig. 9a), salinity decreased with distance from the front, suggesting continued freshening toward shore. This contrasts with the salinity patterns farther from the river mouth at transect IV, for which salinity generally increased toward shore to levels near the ambient offshore salinities (Fig. 10e–h).

Further insights into the patterns of plume salinity can be gained from the CTD casts along transects II and III on 9 June (Fig. 11). Initially the plume was observed to be less than 1 m thick and spreading in both directions from the river mouth (Fig. 11a–d). However, as the plume bent over toward the east it was observed to mix deeper, resulting in plume depths of over 3 m and weaker vertical gradients in salinity (Fig. 11f–h).

Consistent with the surface salinity measurements reported above, the greatest salinity anomalies for the near-river mouth transect III were close to shore rather than at the front. This can be observed in the three final series of CTD casts (Fig. 12), for which the data are shown as the thickness of the freshwater anomaly (d_{fw}), which is calculated by computing the integrated reduction in salinity from each profile:

$$d_{fw} = \int_0^h \frac{(S_0 - S(z))}{S_0}\, dz \tag{3}$$

where S_0 is the ambient seawater salinity (31.3 psu), $S(z)$ is the measured salinity at depth, z, and the integration occurs over the entire water column (h).

Along transect III the values of d_{fw} were consistently greater in the core of the plume than adjacent to the plume front (Fig. 12). For example, at 19:20 the calculated values of d_{fw} in the plume ranged from 45 to 96 cm, with the maximum near the shoreline and a value of 51 cm immediately behind the front (Fig. 12c).

Thus, during accelerating alongshore flow the plume bent over toward the east and mixed deeper into the water column both in the core of the plume and along the front, resulting in an increase in

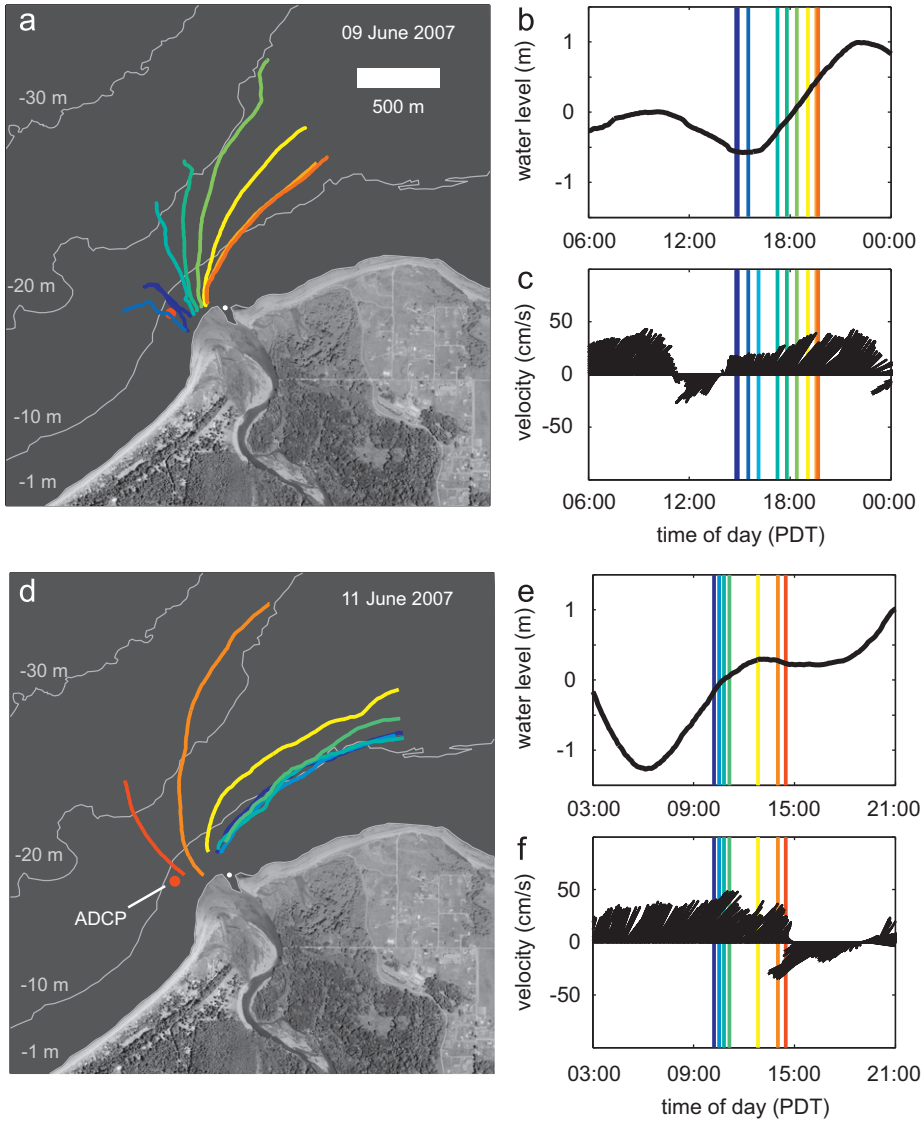

Fig. 7. The location of the westernmost plume front on two separate days during alongshore current acceleration (a)–(c) and deceleration (d)–(f). Fronts are shown in (a) and (d) with colored lines. Matching colors represent the water level observations (b, e) and surface (upper 2 m) currents (c, f) at the moored ADCP site W (shown with red dot in (a) and (d)). The river mouth bar is shown with a white dot.

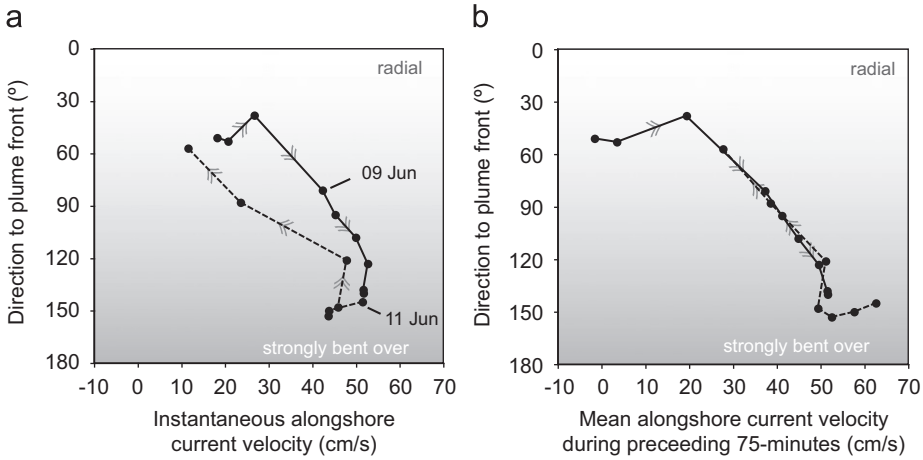

Fig. 8. The relation between alongshore surface current velocity (mean of the upper 2 m) and the location of the westernmost plume front on 9 June (solid) and 11 June (dashed) 2007 (cf. Fig. 7). Direction to the plume front was defined by river mouth (shown with a white dot in Fig. 7) and the location of the plume front at 500 m linear distance from the mouth: (a) instantaneous velocity showing hysteresis between the accelerating and decelerating phases and (b) mean alongshore current velocity during the preceding 75-min.

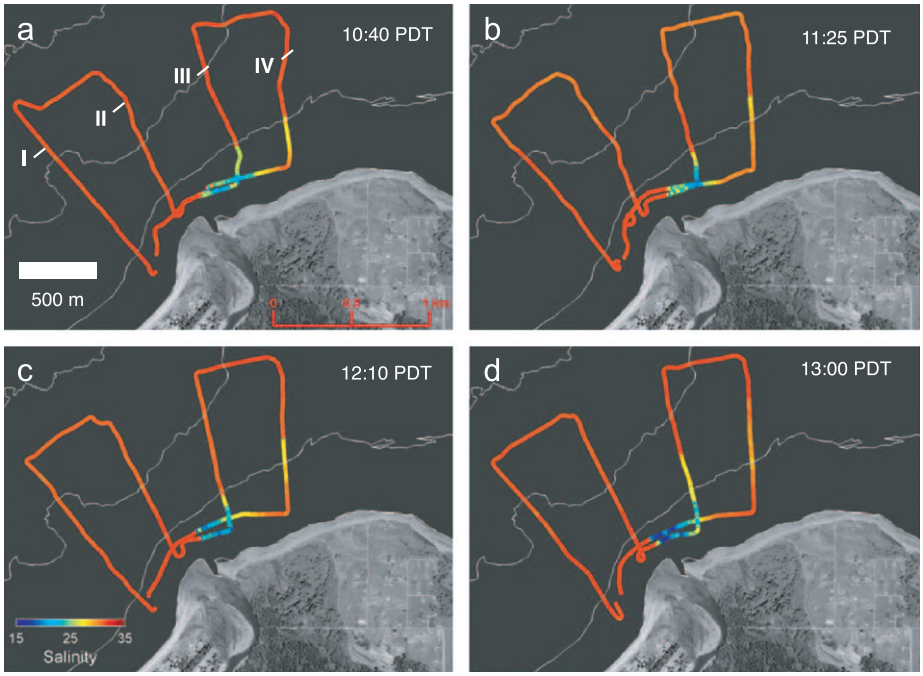

Fig. 9. A time-series of surface salinity measured off the RV *Karluk*'s bow at ~0.4 m depth on 11 June 2007. The across-shore transects are denoted with roman numerals (I–IV) in (a) and details of transects III and IV are shown in Fig. 10.

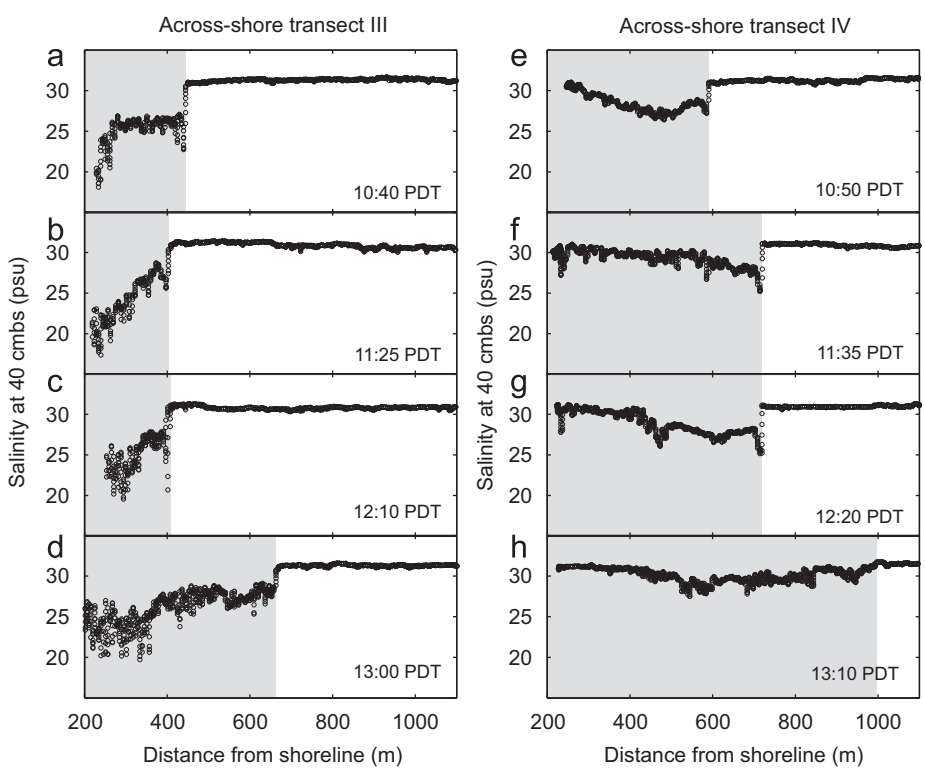

Fig. 10. Surface water salinity measurements across the plume front at transects III and IV (see Fig. 9a for locations). Measurements were taken at ~40 cm below the water surface (cmbs), and observations within the plume as defined by the plume front are shown in the shaded region. All transects except (h) show strong salinity gradients of 3–5 PSU at the plume front.

d_{fw} across the entire plume (Fig. 13). For example, computed values of d_{fw} along transect III were observed to triple during the accelerating flow of 9 June (Fig. 13).

The combination of d_{fw} and plume extent from these surveys allows for the estimation of the mean alongshore velocity component of the buoyant plume water (u_{p-al}) using a mass balance of freshwater by

$$u_{p-al} = \frac{Q}{w_p d_{fw}} \tag{4}$$

where Q is the river discharge (m^3/s), w_p is the width of the plume (m), and d_{fw} is the mean freshwater thickness (m). We calculated

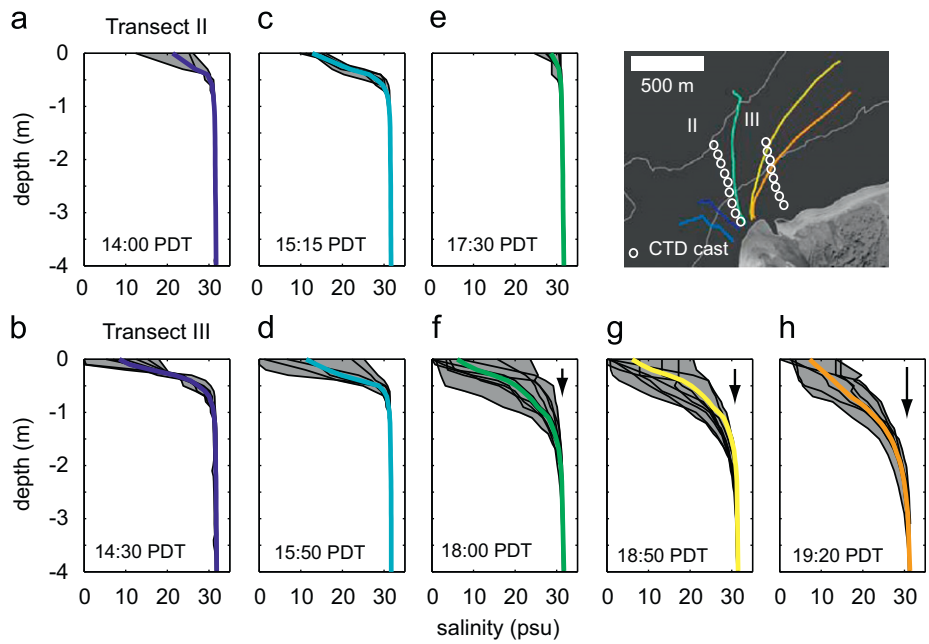

Fig. 11. A series of salinity versus depth measurements for two across-shore transects. Inset map shows the location of the transects and the mapped plume positions on 9 June 2007. Each figure includes all salinity profiles (black lines), the range of salinity observations (gray shading), and the profile mean (color lines). Matching colors in inset map represent plume fronts measured at approximately the same time. Only data within the plume are presented, except for the final transect along II (17:30 PDT), which lies entirely outside of the plume. Arrows on transect III emphasize the deepening of the plume with time.

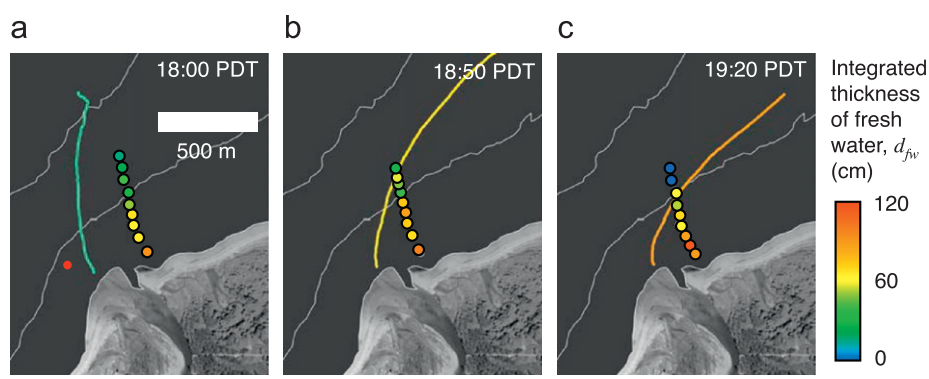

Fig. 12. Integrated thickness of fresh water (d_{fw}) from reduced salinity in the river plume along transect III (see text for definitions). The location of the ADCP is shown with a red dot in (a).

u_{p-al} for two transect III surveys for which CTD casts were obtained fully across the plume (18:50 and 19:20; Fig. 12b and c). These $u_{p\text{-}al}$ values are 20–25 cm/s, which are roughly half of the measured alongshore velocities measured at the adjacent ADCP station (Fig. 13b), which suggests net convergence between the plume and adjacent surface waters.

The alongshore component of the buoyancy-related velocity of the plume can be estimated by the difference of the alongshore current and u_{p-al}, and we calculate it to be 25–30 cm/s and directed opposing the alongshore flow (i.e., toward the west). These values can be compared to theoretical buoyancy velocities computed from buoyancy anomalies assuming hydrostatic conditions and applying Bernoulli's equation (e.g., Geyer et al., 2000). Such computations suggest frontal speeds of 31 and 50 cm/s during 18:50 and 19:20, respectively, with peak buoyancy velocities of 64–70 cm/s in the core of the plume. For a direct comparison with the mass balance computed buoyancy velocities of 25–30 cm/s, we transform the mean theoretical buoyancy velocities (50 and 56 cm/s, respectively) into the alongshore components using the angle between the front and the local bathymetry (30° and 25°, respectively). This results in alongshore components of the buoyancy velocity of ~25 cm/s, which are roughly equivalent to the 25–30 cm/s values reported above.

Summarizing, these results suggest that: (i) as the alongshore current accelerates, freshwater is mixed deeper resulting in greater buoyancy anomalies and velocities, (ii) within 500 m of the river mouth the lowest salinities and greatest freshwater thicknesses were measured in the core of the plume away from the front, (iii) this, combined with estimates of buoyancy velocities, suggest that there is net convergence toward the front in this inner section of the plume, and (iv) the estimates of plume velocities suggest that buoyancy contributes significantly to plume behavior, which will result in considerable shear along the plume's front and basal interface.

5. Discussion

5.1. Dynamical classification of the Elwha plume

The Elwha River forms a buoyant plume on the western side of its deltaic headland, which makes it subject to transient eddies and

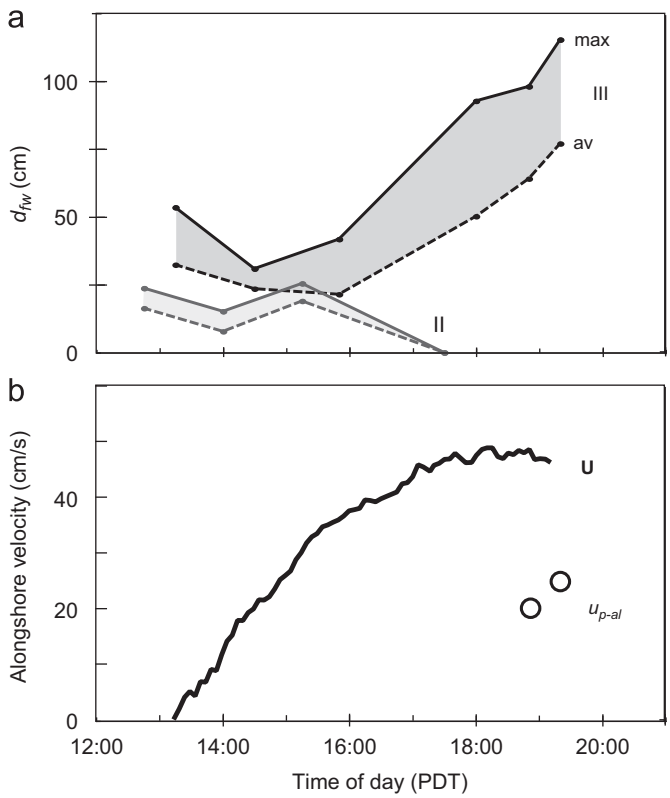

Fig. 13. The evolution of (a) the integrated thickness of freshwater (d_{fw}) with time on 9 June 2007 for across-shore transects II (gray) and III (black) as (b) the alongshore current of the surface water (U) accelerated toward the east. For each transect the average and maximum values of fresh water anomaly are shown (av, max). The computed alongshore component of the plume velocity (u_{p-al}) is also shown in (b) with round symbols. See the inset in Fig. 11 for station locations.

asymmetric flow. Further assessment of this plume can be made using Garvine's (1995) dynamical classification system that utilizes the plume Kelvin number (K):

$$K = \frac{\gamma L f}{c} \tag{5}$$

where γL is the across-shore length scale, f is the Coriolis parameter, and c is the internal wave phase speed across the vertical density gradient of the plume. From our observations of the Elwha River plume, we suggest that γL is $\sim$1000 m and f is $\sim 10^{-4}$ s^{-1}. Garvine (1995) suggests that c can be approximated by

$$c = \sqrt{g' D} \tag{6}$$

where g' is the reduced gravity, which is equivalent to $g(\Delta\rho/\rho_0)$, $\Delta\rho$ is the average density difference between the plume and ambient waters, and D is the mean plume thickness. We suggest that $\Delta\rho$ is $\sim$12 kg/m^3 and D varied between 1 and 3 m, which results in c having a range of 0.3–0.6 m/s.

Solving for K, we find that it has a range of 0.2–0.3, which would classify the Elwha as a "small-scale" (or "Case 1") system as defined by Garvine (1995), which may also be referred to as a "narrow" plume. The across-shore scale for these kinds of plumes are small compared to the Rossby radius, thus the effects of the Coriolis force on the momentum balance should be negligible.

There are two important implications of this "small-scale" or "narrow" classification. First, rotational features such as an unsteady plume "bulge" offshore of the river mouth (e.g., Horner-Devine, 2009) and geostrophic or semi-geostrophic currents (e.g., Fong and Geyer, 2002) should not be expected within the 1 km region we sampled, although they may occur further offshore of this region. In contrast, Garvine (1995) suggests that small-scale plumes should have strong boundary fronts that are similar to internal hydraulic jumps, and that advection of the plume would depend upon: (i) the plume's baroclinic forcing, (ii) wind stress, and (iii) basal stress from the local current.

Our results from the Elwha River plume are consistent with Garvine's (1995) model, because strong fronts were observed and the plume responded strongly to the local current and to the plume's baroclinic forcing. Under the physical conditions of our plume observations, namely constant river discharge and low wind stress, it should be expected that the plume behavior would be strongly related to the local current, such as suggested above. Although our observations do suggest that the "small-scale" plume of the Elwha River responds strongly to the local flow, there is a significant delay (O(1 h)) before a steady response is achieved to changes in this basal stress. This is consistent with a lagged response of buoyant plumes to wind stress, although the time scales of wind responses have been observed to be several hours (Whitney and Garvine, 2005; Warrick et al., 2007).

The second implication of the "small-scale" classification is that the Elwha River plume should respond in a symmetrical manner to alongshore currents of equal magnitude but opposing direction, because there is negligible influence from rotation near the river mouth. We will explore this further with a simple conceptual model.

5.2. Conceptual model of the Elwha plume

Our observations that the physical behavior of the Elwha River plume responded to alongshore flow conditions are certainly not unique. For example, Garvine (1974) clearly showed that tidal currents provided a fundamental control on the direction and extent of the Connecticut River plume. Thus, we will explore a simple conceptual model of the plume behavior considering first only the effects of alongshore currents in the immediate river mouth region. We note that far-field (> 1 km) currents and plume behavior would likely be unrelated owing to non-uniform currents (e.g., shear and eddies) and perhaps rotation, so this analysis will be applicable only to the near-field (i.e., within $\sim$1 km). We proceed, however, because this region can be very important for sediment dispersal patterns as noted by Hill et al. (2007) and as described below.

Because our observations suggest that the position of the near-field plume front was related to the mean local alongshore velocity (u_{av}) during the preceding O(1 h), we suggest that our flow records from 2006 can be used to evaluate the relative frequency of various plume conditions in both flood-like and ebb-like states. This simple model does not include the effects of variations in discharge or wind stress, although we discuss these topics more fully below. The histogram of u_{av} calculated using a 75-min window for the 96-day West site ADCP record is shown in Fig. 14, and we include five general plume conditions based upon u_{av}. "Strongly bent over"

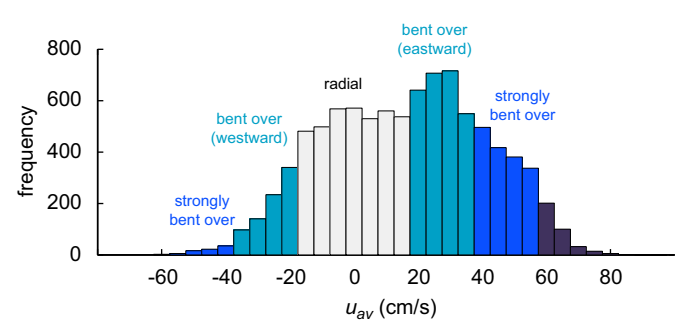

Fig. 14. Histogram of the time-averaged alongshore current velocity (u_{av}) at the West ADCP site during the 2006 deployment. Owing to the strong effect of u_{av} on observed plume behavior, regions of the histogram are highlighted to show expected behavior.

plume behavior is defined to be when the front extends back completely past the river mouth, which occurs when u_{av} is greater than ~40 cm/s (cf. Fig. 8b). "Bent over" plume behavior has a well-defined front that does not extend back fully past the river mouth, and we approximate this to occur for u_{av} in the range 20–40 cm/s. For u_{av} less than 20 cm/s, we suggest the plume spreads in a more radial manner (Garvine, 1984).

The results of this simple exercise suggest that for the discharge range and coastal conditions we observed, the Elwha River plume would be bent over toward the east half of the time (~50%; Fig. 14). The next most frequent condition (~41% of the record) is a radial-spreading plume owing to weak alongshore currents near the river mouth (Fig. 14). We predict that the most infrequent condition of the Elwha River plume is bent over toward the west, which is predicted to occur less than 10% of the time.

The reason that these eastward-directed plumes are common is the effect of the headland on flow conditions (Fig. 15). The eddy formed in the lee of the headland during the regional ebb is responsible for the dominance of these eastward flow conditions at the river mouth (Fig. 15b). Radial dispersal would be expected during slack currents, and a westward-directed plume (not shown in Fig. 15) is most likely during the early portion of the regional ebb, before the flow-separation occurs (cf. Fig. 5a).

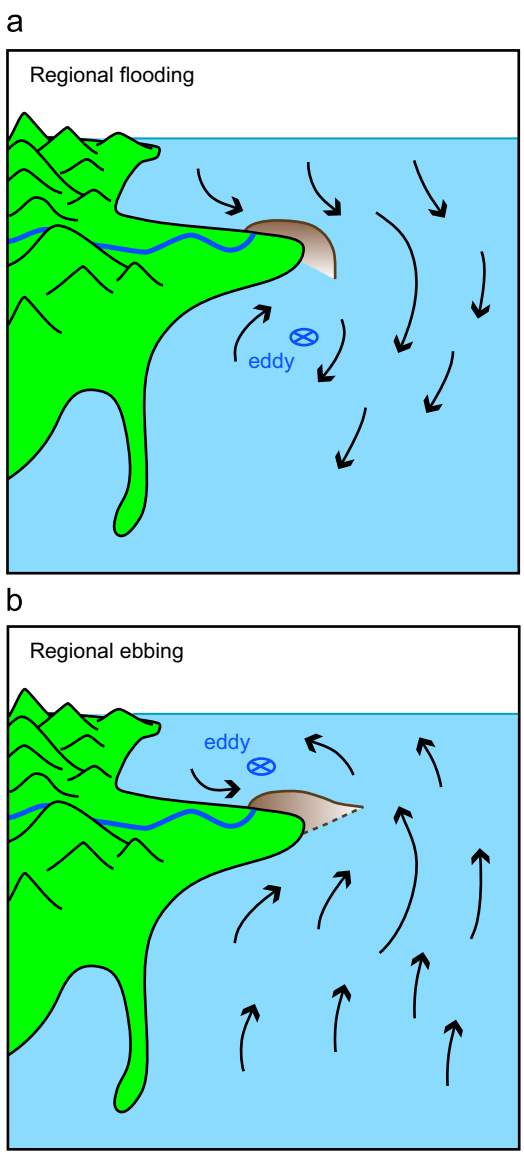

Fig. 15. Conceptual model of the behavior of the Elwha River plume (brown shading) during (a) flooding and (b) ebbing current conditions. The headland-induced eddy under each circumstances is shown with a round symbol. During regional ebbing (b) there is likely a front formed immediately offshore of the headland at the point of flow separation (dashed line).

This simplified conceptual model of the near-field plume does not include the effects of variations in discharge or wind, both of which can greatly influence plume extent and behavior (Garvine, 1974; Whitney and Garvine, 2005). The effect of discharge is to modify the rate of buoyancy flux, and under high discharge conditions this would greatly expand the extent of the plume. Discharge may also be regulated by tidal pumping of the estuary if the tidal prism is large with respect to river discharge (e.g., Pritchard and Huntley, 2006; Hickey et al., 2010). Using the area of the tidally influenced river mouth (~100,000 m^2; cf. Curran et al., 2009), and the modal and maximum rates of absolute water level change from the west ADCP pressure sensor (0.1 and 0.2 m/s), the inflow and outflow rates related to the tidal prism are estimated to be commonly ~10 m^3/s and rarely up to 20 m^3/s. Although these tidal-related flow rates are lower than the discharge conditions monitored here (60 m^3/s) and mean and flood discharge rates from the river (40 and 400 m^3/s, respectively), they certainly can overwhelm the summer baseflow conditions that are commonly ~10 m^3/s (Fig. 3). During these low discharge conditions, we would expect more river discharge to exit the river mouth under the falling water levels. We also acknowledge that a better understanding for estuarine mixing characteristics (e.g., presence and absence of well stratified and/or well mixed zones) within the river mouth will be needed to better evaluate this tidal pumping effect.

Finally, buoyant plume behavior for a "small-scale" plume such as the Elwha will be strongly influenced by wind (Garvine, 1995; Fong and Geyer, 2001; Whitney and Garvine, 2005). Unfortunately, very little wind data exists for the central Strait of Juan de Fuca, which hampers our ability to characterize this effect. Furthermore, all of our June 2007 plume surveys were made during low wind conditions (less than 10 m/s). However, the ADCP record used to generate the conceptual model in Fig. 14 included many western wind events during this winter to spring record as suggested by regular low period wave events (Warrick et al., 2009). As noted in Section 2 above, regional winds can be strong and are commonly westerly in the study area. This should produce a plume that would be more likely to bend over toward the east than observed in our surveys. Thus, the effects of the regular westerly winds are hypothesized to increase the intensity and duration of eastward bent-over conditions.

5.3. Implications for sediment dispersal

The pending removal of dams on the Elwha River will introduce millions of cubic meters of suspended sediment into the Strait of Juan de Fuca and restore regular inputs of upper watershed suspended sediment to the river mouth (Duda et al., 2008; Konrad, 2009). Thus, it is expected that this restoration will result in increased turbidity and sediment fluxes throughout the Elwha River delta coastal zone.

An initial assessment of the suspended-sediment transport in the near-field plume can be shown with an exploration of mass balances and scaling for fine sediment (silt and clay). We do not consider sand here, owing to the more rapid settling velocities expected for this material. The time for which freshwater parcels reside in the 1 km near-field plume region can be estimated by the ratio of this distance to the average plume speed (20–50 cm/s), resulting in a 2000–5000 s residence time (i.e., approximately 0.5–1.5 h). The average depth of suspended sediment settling over this distance is equivalent to the product of the sediment settling

velocity (w_s) and the residence time. Fine sediment will commonly flocculate in coastal river plumes resulting in mean w_s of approximately 1 mm/s (Hill et al., 2007). This results in total fine sediment settling distances of 2–5 m in this near-field plume, which is roughly equivalent to or slightly greater than the observed plume thicknesses of 1–3 m. This suggests that half or more of the mass of fine sediment discharged will settle from the buoyant plume within this 1 km near-field region.

We note that under the extreme sediment loading expected during floods following dam removal, the river suspended-sediment concentrations will exceed several 10's of g/l (Konrad, 2009). Under these conditions, it is likely that fine sediment w_s may approach 10 or more mm/s, owing to the effects of convective instabilities (McCool and Parsons, 2004; Warrick et al., 2008), or under extreme conditions in which the river suspended-sediment concentrations are >40 g/l, the discharge will be negatively buoyant resulting in a hyperpycnal gravity currents (Mulder and Syvitski, 1995). Under these conditions, it should be expected that fine sediment pathways would rapidly converge to the seafloor within 1 km of the mouth (e.g., Warrick et al., 2008).

This does not mean that the nearshore waters beyond a kilometer from the river mouth will be free of suspended sediment and turbidity. On the contrary, it is well recognized that the settling velocities of fine sediment in buoyant plumes have broad distributions owing the diversity of flocculated and individual particles present (Hill et al., 2007), and that may take 10–40 h for adequate settling of fine sediment for optical properties of the plume to indistinguishable from ambient coastal waters. In the case of the Elwha River plume, this would suggest that river-derived turbidity could extend several kilometers away from the river mouth (M2 tidal exclusions are $\sim$10 km). Thus, although the majority of the suspended sediment is expected to settle from the buoyant plume near the river mouth, the effects of turbidity on optical properties of the plume should extend much further. This will likely have implications to the amount of photosynthetically active radiation, or PAR, available to algae and other primary producers in region during and after the dam removal process.

5.4. Broader implications

Beyond the regional setting of the Strait of Juan de Fuca and the Elwha River, there are several broader implications of these results to the understanding of buoyant river plumes. Firstly, it was shown that coastal topographic features were able to influence the physical behavior of a buoyant river plume. In the case of the Elwha River, this topographic effect was somewhat straightforward owing to the nature of the deltaic headland and the oscillatory flow—a coastal setting that has been rather well studied (e.g., Signell and Geyer, 1991). As plume studies examine smaller and smaller river settings – largely in response to the importance of these systems in global geochemical cycles and local water quality – these topographic effects on plume behavior may be found to be more common. We hypothesize that this would result from the more irregular coastal settings near small rivers, especially along active tectonic margins, and also because topographic features of a specific size will have a large effect on a small plume while having a negligible effect on a large plume.

It is also valuable to compare our frontal and buoyancy observations to those observed previously and those proposed in numerical models. First, the plume front and head were observed to occur over short distance scales (less than 5 and $\sim$20 m, respectively), consistent with the observations of many including Trump and Marmorino (2003) and O'Donnell et al. (2008). As pointed out by O'Donnell et al. (2008), the primitive equation models that are commonly used to simulate river plumes are not constructed to resolve these spatial scales. In fact most recent applications of these models have focused away from the frontal dynamics and more on plume spreading and mixing (e.g., MacDonald et al., 2007; Hetland and MacDonald, 2008). Although these topics are relevant to settings such as the Elwha River (see below), they generally avoid insights into the frontal behavior, which is a defining feature of many small-scale plumes such as the Elwha (Garvine, 1995).

Our results are generally consistent with another set of river plume models, those that treat the plume front as a free boundary in an attempt to better characterize the frontal dynamics (see O'Donnell, 1993, for a review)—especially when considering these dynamics in strong alongshore flows. However, our results suggest that the buoyancy structure within the core of the plume may deviate somewhat from these models. Our observations suggest that within $\sim$500 m of the river mouth there was a "core" of greatest freshwater thickness away from the plume front (Figs. 10 and 13) and significant convergence of plume water toward the front. This "core" is not observed in the frontal models described in O'Donnell (1993), perhaps owing to the assumed uniform distribution of river outflow in these models. We hypothesize that the absolute effect of these differences on plume extent and behavior is minor.

Lastly, our observations reveal that mixing during strong alongshore flow was vigorous both along the front and on the plume's basal boundary. Mixing along the front was recognized from the easily observed and measured surface water convergence and regular $\sim$2 m cuspate forms with 0.1–1 m eddies along the front. However, mixing also appears to be important along the plume's base, owing to the 1–2 m deepening of isohalines during accelerating alongshore flow (Fig. 11). We note that this deepening occurred both at the front and also in the plume core, the latter of which likely had not been mixed through the frontal region as discussed above. Thus, future investigations of river plumes in high shear settings such as shown here should not assume that mixing only occurs through either frontal (e.g., Pritchard and Huntley, 2006) or basal mixing (e.g., Hetland, 2009) alone, because both may play integral parts to the plume behavior.

6. Conclusions

The Elwha River of Washington discharges on the western side of its deltaic headland in strongly oscillatory flow. This oscillatory tidal flow produces flow separation and transient eddies around the delta. These flow patterns strongly influence the river plume, which bends over during strong alongshore flow, and is expected to do so more frequently in the eastward direction. We suggest that these conditions will influence the initial direction of water and sediment transport from the river. These findings are especially relevant to a pending dam removal project that will produce exceptional sediment fluxes to the coastal zone. This work shows that topographic features may substantially influence the dispersal behavior of river plumes, and we suggest that these types of interactions may be much more common for the dispersal of water and materials from the smaller rivers of the world.

Acknowledgements

We would like to thank Joanne Ferreira, Jamie Grover, Gerry Hatcher, Guy Gelfenbaum, Hal Williams, Dave Gonzales, and Chris Curran for their assistance with instrumentation and field activities. This paper was improved substantially by comments from Amy Draut, Jessica Lacy and two anonymous reviewers. This work was funded by the Coastal Habitats in Puget Sound (CHIPS) project within the Coastal and Marine Geology Program of the USGS.

References

Bertotti, G., Mayergoyz, I.D., 2006. The Science of Hysteresis (3-volume Set). Academic Press, Oxford, UK, 2160 pp.

Chen, F., MacDonald, D.G., Hetland, R.D., 2009. Lateral spreading of a near-field river plume: observations and numerical simulations. Journal of Geophysical Research 114, C07013. doi:10.1029/2008JC004893.

Childers, D., Kresch, D.L., Gustafson, S.A., Randle, T.J., Melena, J.T., Cluer, B., 2000. Hydrologic data collected during the 1994 Lake Mills drawdown experiment, Elwha River, Washington. US Geological Survey Water-Resources Investigation Report 99-4215, 115 pp.

Curran, C.A., Konrad, C.P., Dinehart, R.L., Moran, E.H., 2009. Bank topography, bathymetry, and current velocity of the Lower Elwha River, Clallam County, Washington, May 2006. U.S. Geological Survey Data Series 363, 12 pp.

Duda, J.J., Freilich, J.E., Schreiner, E.G., 2008. Baseline studies in the Elwha River ecosystem prior to dam removal: introduction to the special issue. Northwest Science 82, 1–12.

Fong, D.A., Geyer, W.R., 2001. Response of a river plume during an upwelling favorable wind event. Journal of Geophysical Research 106, 1067–1084.

Fong, D.A., Geyer, W.R., 2002. The alongshore transport of freshwater in a surface-trapped river plume. Journal of Physical Oceanography 32, 957–972.

Foreman, M., Sutherland, G., Cummins, P.F., 2004. M2 tidal dissipation around Vancouver Island: an inverse approach. Continental Shelf Research 24, 2167–2185.

Garvine, R.W., 1974. Physical features of the Connecticut River outflow during high discharge. Journal of Geophysical Research 79, 831–846.

Garvine, R.W., 1984. Radial spreading of buoyant, surface plumes in coastal waters. Journal of Geophysical Research 89, 1989–1996.

Garvine, R.W., 1995. A dynamical system for classifying buoyant coastal discharges. Continental Shelf Research 15, 1585–1596.

Garvine, R.W., Monk, J.D., 1974. Frontal structure of a river plume. Journal of Geophysical Research 79, 2251–2259.

Gelfenbaum, G., Stumpf, R.P., 1993. Observations of currents and density structure across a buoyant plume front. Estuaries 16, 40–52.

Geyer, W.R., Signel, R., 1990. Measurements of tidal flow around a headland with a shipboard acoustic doppler current profiler. Journal of Geophysical Research 95, 3189–3197.

Geyer, W.R., Hill, P., Milligan, T., Traykovski, P., 2000. The structure of the Eel River plume during floods. Continental Shelf Research 20, 2067–2093.

Geyer, W.R., Hill, P.S., Kineke, G.C., 2004. The transport, transformation and dispersal of sediment by buoyant coastal flows. Continental Shelf Research 24, 927–949.

Gilbert, J.D., Link, R.A., 1995. Alluvium distribution in Lake Mills, Glines Canyon Project, and Lake Aldwell, Elwha project, Washington. Boise, Idaho, Bureau of Reclamation, Elwha Technical Series PN-95-459, 61 pp.

Hetland, R.D., 2005. Relating river plume structure to vertical mixing. Journal of Physical Oceanography 35, 1667–1688.

Hetland, R.D., MacDonald, D.G., 2008. Spreading in the near-field Merrimack river plume. Ocean Modeling 21, 12–21.

Hetland, R.D., 2009. The effects of mixing and spreading on density in near-field river plumes. Dynamics of Atmospheres and Oceans 49, 37–53.

Hickey, B.M., Kudela, R.M., Nash, J.D., Bruland, K.W., Peterson, W.T., MacCready, P., Lessard, E.J., Jay, D.A., Banas, N.S., Baptista, A.M., Dever, E.P., Kosro, P.M., Kilcher, L.K., Horner-Devine, A.R., Zaron, E.D., McCabe, R.M., Peterson, J.O., Orton, P.M., Pan, J., Lohan, M.C., 2010. River influences on shelf ecosystems: Introduction and synthesis. Journal of Geophysical Research 115, C00B17, doi:10.1029/2009JC005452.

Hill, P.S., Fox, J.M., Crockett, J., Curran, K.J., Drake, D.E., Friedrichs, C.T., Geyer, W.R., Milligan, T.G., Ogston, A.S., Puig, P., Scully, M.E., Traykovski, P., Wheatcroft, R.A., 2007. Sediment delivery to the seabed on the Eel River continental margin. In: Nittrouer, C.A. (Ed.), Continental Margin Sedimentation: Transport to Sequence. International Association of Sedimentologists. Blackwell, pp. 560.

Holbrook, J.R., Muench, R.D., Kachel, D.G., Wright, C., 1980. Circulation in the Strait of Juan de Fuca: recent oceanographic observations in the eastern basin. NOAA Technical Report PMEL 33, 42 pp.

Horner-Devine, A.R., 2009. The bulge circulation in the Columbia River plume. Continental Shelf Research 29, 234–251. doi:10.1016/j.csr.2007.12.012.

Kilcher, L.F., Nash, J.D., 2010. Structure and dynamics of the Columbia River tidal plume front. Journal of Geophysical Research 115, C05S90. doi:10.1029/2009JC006066.

Kineke, G.C., Woolfe, K.J., Kuehl, S.A., Milliman, J.D., Dellapenna, T.M., Purdon, R.G., 2000. Sediment export from the Sepik River, Papua New Guinea: evidence for a divergent sediment plume. Continental Shelf Research 20, 2239–2266.

Kloehn, K.K., Beechie, T.J., Morley, S.A., Coe, H.J., Duda, J.J., 2008. Influence of dams on river-floodplain dynamics in the Elwha River, Washington. Northwest Science 82, 224–235.

Konrad, C.P., 2009. Simulating the recovery of suspended sediment transport and river-bed stability in response to dam removal on the Elwha River, Washington. Ecological Engineering 35, 1104–1115.

Lange, O.S., 1999. The wind came all ways: a quest to understand the winds, waves and weather in the Georgia Basin. Environment Canada, Vancouver, BC, 123 pp.

Lange, O.S., 2003. The veil of chaos: living with weather along the British Columbia coast. Environment Canada, Vancouver, BC, 198 pp.

Luketina, D.A., Imberger, J., 1987. Characteristics of a surface buoyant jet. Journal of Geophysical Research 92, 5435–5447.

Masson, D., Cummins, P.F., 2004. Observations and modeling of seasonal variability in the Straits of Georgia and Juan de Fuca. Journal of Marine Research 62, 491–516.

MacDonald, D.G., Geyer, W.R., 2004. Turbulent energy production and entrainment at a highly stratified estuarine front. Journal of Geophysical Research 109, C05004. doi:10.1029/2003JC002094.

MacDonald, D.G., Goodman, L., Hetland, R.D., 2007. Turbulent dissipation in a near-field river plume: a comparison of control volume and microstructure observations with a numerical model. Journal of Geophysical Research 112, C07026. doi:10.1029/2006JC004075.

McCabe, R., MacCready, P., Pawlak, G., 2006. Form Drag due to flow separation at a headland. Journal of Physical Oceanography 36, 2136–2152.

McCool, W.W., Parsons, J.D., 2004. Sedimentation from buoyant fine-grained suspensions. Continental Shelf Research 24, 1129–1142.

Mertes, L.A.K., Warrick, J.A., 2001. Measuring flood output from 110 coastal watersheds in California with field measurements and SeaWiFS. Geology 29, 659–662.

Milligan, T.G., Hill, P.S., Law, B.A., 2007. Flocculation and the loss of sediment from the Po River plume. Continental Shelf Research 27, 309–321. doi:10.1016/j.csr.2006.11.008.

Milliman, J.D., Syvitski, J.P.M., 1992. Geomorphic tectonic control of sediment discharge to the ocean—the importance of small mountainous rivers. Journal of Geology 100, 525–544.

Mulder, T., Syvitski, J.P.M., 1995. Turbidity currents generated at river mouths during exceptional discharges to the world oceans. Journal of Geology 103, 285–299.

O'Donnell, J., 1990. The formation and fate of a river plume: a numerical model. Journal of Physical Oceanography 20, 551–559.

O'Donnell, J., 1993. Surface fronts in estuaries: a review. Estuaries 16, 12–39.

O'Donnell, J., Marmorino, G.O., Trump, C.L., 1998. Convergence and downwelling at a river plume front. Journal of Physical Oceanography 28, 1481–1495.

O'Donnell, J., Ackleson, S.G., Levine, E.R., 2008. On spatial scales of a river plume. Journal of Geophysical Research 113, C04017. doi:10.1029/2007JC004440.

Piñones, A., Valle-Levinson, A., Narvaez, D.A., Vargas, C.A., Navarrete, S.A., Yuras, G., Castilla, J.C., 2005. Wind-induced diurnal variability in river plume motion. Estuarine, Coastal and Shelf Science 65, 513–525.

Pritchard, M., Huntley, D.A., 2006. A simplified energy and mixing budget for a small river plume discharge. Journal of Geophysical Research 111, C03019. doi:10.1029/2005JC002984.

Randle, T. J., Young, C. A., Melena, J. T., Ouellette, E. M., 1996. Sediment analysis and modeling of the river erosion alternative. Elwha Technical Series PN-95-9, US Department of the Interior, Bureau of Reclamation, Boise, ID.

Saunders, P.M., 1981. Practical conversion of pressure to depth. Journal of Physical Oceanography 11, 573–574.

Signell, R.P., Geyer, W.R., 1991. Transient eddy formation around headlands. Journal of Geophysical Research 96, 2561–2576.

Thomson, R.E., Mihály, S.F., Kulikov, E.A., 2007. Estuarine versus transient flow regimes in Juan de Fuca Strait. Journal of Geophysical Research 112, C09022. doi:10.1029/2006JC003925.

Trump, C.L., Marmorino, G.O., 2003. Mapping small-scale along-front structure using ADCP acoustic backscatter range-bin data. Estuaries 26, 878–884.

Warrick, J.A., DiGiacomo, P.M., Weisberg, S.B., Nezlin, N.P., Mengel, M., Jones, B.H., Ohlmann, J.C., Washburn, L., Terrill, E.J., Farnsworth, K.L., 2007. River plume patterns and dynamics within the Southern California Bight. Continental Shelf Research 27, 2427–2448.

Warrick, J.A., Xu, J., Noble, M.A., Lee, H.J., 2008. Rapid formation of hyperpycnal sediment gravity currents offshore of a semi-arid California river. Continental Shelf Research 28, 991–1009. doi:10.1016/j.csr.2007.11.002.

Warrick, J.A., George, D.A., Gelfenbaum, G., Kaminsky, G., Beirne, M., 2009. Beach morphology and change along the mixed grain-size delta of the Elwha River, Washington. Geomorphology 111, 136–148.

Whitney, M.M., Garvine, R.W., 2005. Wind influence on a coastal buoyant outflow. Journal of Geophysical Research 110, C3014. doi:10.1029/2003JC002261.

Wheatcroft, R.A., Goñi, M.A., Hatten, J.A., Pasternack, G.B., Warrick, J.A., 2010. The role of effective discharge in the ocean delivery of particulate organic carbon by small, mountainous river systems. Limnology and Oceanography 55, 161–171.

Wolanski, E., Hamner, W.M., 1988. Topographically controlled fronts in the ocean and their biological influence. Science 241, 177–181.

Wright, L.D., Coleman, J.M., 1971. Effluent Expansion and interfacial mixing in the presence of a salt wedge, Mississippi River Delta. Journal of Geophysical Research 76, 8649–8661.

Wright, L.D., Friedrichs, C.T., 2006. Gravity-driven sediment transport on continental shelves: a status report. Continental Shelf Research 26, 2092–2107. doi:10.1016/j.csr.2006.07.008.

Wunderlich, R.C., Winter, B.D., Meyer, J.H., 1994. Restoration of the Elwha River ecosystem. Fisheries 19, 11–19.

Yankovsky, A.E., Chapman, D.C., 1997. A simple theory for the fate of buoyant coastal discharges. Journal of Physical Oceanography 27, 1386–1401.